Spatial Proximity of the HIV-1 Nucleocapsid Protein Zinc Fingers Investigated by Time-Resolved Fluorescence and Fluorescence Resonance Energy Transfer†

Y. Mély,*,‡ N. Jullian,§ N. Morellet,§ H. De Rocquigny,§ C. Z. Dong,§ E. Piémont,‡ B. P. Roques,§ and D. Gérard‡

Laboratoire de Biophysique de la Faculté de Pharmacie, CNRS UA 491, Université Louis Pasteur, Strasbourg I, BP 24, 67401 Illkirch Cedex, France, and Département de Chimie Organique, INSERM U266, CNRS UA 498, UFR des Sciences Pharmaceutiques et Biologiques, 4 avenue de l'Observatoire, 75270 Paris Cedex 06, France

Received June 10, 1994; Revised Manuscript Received August 8, 1994®

ABSTRACT: The three-dimensional structure of peptides encompassing the two zinc-saturated finger motifs of the nucleocapsid protein NCp7 of HIV-1 has been reported by several groups. Whereas the folded structures of the finger motifs were in good agreement, discrepancies existed concerning their spatial relationship since the fingers were found either close to each other [Morellet, N., Jullian, N., De Rocquigny, H., Maigret, B., Darlix, J. L., & Roques, B. P. (1992) *Embo J. 11*, 3059–3065] or independently folded [Omichinski, J. G., Clore, G. M., Sakaguchi, K., Appella, E., & Gronenborn, A. M. (1991) *FEBS Lett. 292*, 25–30; Summers, M. F., Henderson, L. E., Chance, M. R., Bess, J. W., Jr., South, T. L., Blake, P. R., Sagi, I., Perez-Alvarado, G., Sowder, R. C., III, Hare, D. R., & Arthur, L. O. (1992) *Protein Sci. 1*, 563–574]. As in the interacting finger model, Phe^{16} in the NH_2-terminal finger and Trp^{37} in the COOH-terminal finger were found to be spatially close, the fluorescence properties of the aromatic residues at positions 16 and 37 in the wild-type and two conservatively substituted (12–53)NCp7 peptides were investigated and compared with those of three negative control derivatives where the finger motifs were not in close contact. Direct distance measurements by Tyr-Trp fluorescence resonance energy transfer of the former derivatives yielded a 7–12 Å interchromophore distance range which is clearly inconsistent with the 12.5–18 Å range measured for the negative controls and thus a random orientation of the zinc finger motifs. In keeping with the proximity of the two finger motifs in the former derivatives, a dramatic decrease in both the native Trp^{37} and the conservatively substituted Trp^{16} fluorescence quantum yields, correlated to the appearance of an additional subnanosecond lifetime was observed. Moreover, as expected, the amplitude of Trp local motion in these derivatives was significantly lower than that in the negative controls. Finally, refinement of the distance range measured by fluorescence energy transfer, using the NMR-derived angles of the model with interacting fingers, yielded a mean interchromophore distance of 7.3 ± 0.7 Å, in good agreement with the NMR-deduced distances of this model. Taken together, our data confirmed the spatial proximity of the two finger motifs, a feature that must be of critical importance for the recognition of the target nucleic acids.

All retroviruses encode a gag precursor polyprotein that is, subsequent to viral assembly and budding, processed by the retroviral protease to give several structural proteins, including the nucleocapsid protein (NC).[1] In human immunodeficiency virus type 1 (HIV-1), the nucleocapsid protein NCp15 is derived from the Pr55 gag polyprotein precursor and is ultimately processed into NCp7 and -p6 proteins in the mature HIV virus (Di Marzo Veronese et al., 1987). The processed NCp7 protein is highly basic and contains two Cys-X_2-Cys-X_4-His-X_4-Cys retroviral-type zinc fingers, also referred to as CCHC motifs (Berg, 1986), which have been shown to stoichiometrically bind zinc in mature virus preparations (Bess et al., 1992; Summers et al., 1992).

In the capsid of the HIV-1 virion, NC is thought to stabilize the dimeric RNA genome through formation of a ribonucleoprotein complex (Darlix et al., 1990). *In vitro*, NC has been shown to activate the retroviral RNA dimerization (Darlix et al., 1990) and the annealing of the primer $tRNA_3^{Lys}$ to the initiation site of reverse transcription (Barat et al., 1989), suggesting a critical role for NC in both genomic RNA packaging and reverse transcription. Point mutation experiments strongly suggest that the finger motifs are involved in the control of the viral genomic RNA encapsidation (Aldovini & Young, 1990; Gorelick et al., 1990). In contrast, replacement of both fingers by a Gly-Gly linker does not inhibit the *in vitro* RNA binding and annealing activities of NC, whereas the short basic sequences ^{13}VK and ^{29}RAPRKKG^{35} flanking the first finger are of critical importance in these NCp7 functions (De Rocquigny et al., 1992). Thus, it was suggested that the role of the zinc finger motifs might be to direct spatial recognition by these short basic sequences of specific sites on the viral RNA.

The three-dimensional structures of zinc-saturated (1–55)-NCp7 (Summers et al., 1992) and (13–51)NCp7 (Omichinski et al., 1991; Morellet et al., 1992) have been reported. In all of these structures, the conformations of the zinc finger domains were largely superimposable on those previously reported in the isolated synthetic zinc finger peptides (Summers et al., 1990; South et al., 1991). In contrast, whereas Omichinski et al. (1991) and Summers et al. (1992) found the two finger motifs of NCp7 to be structurally independent, Morellet et al. (1992) proposed the existence of spatial contacts

† This work was supported by grants from the Agence Nationale de la Recherche sur le SIDA, Centre National de la Recherche Scientifique, and Université Louis Pasteur.

* Author to whom proofs and correspondence should be addressed.
‡ Université Louis Pasteur.
§ UFR des Sciences Pharmaceutiques et Biologiques.

® Abstract published in *Advance ACS Abstracts,* September 15, 1994.

[1] Abbreviations: NC, nucleocapsid protein; Hepes, *N*-(2-hydroxyethyl)piperazine-*N'*-2-ethanesulfonic acid; FRET, fluorescence resonance energy transfer.

0006-2960/94/0433-12085$04.50/0

between the two zinc fingers (notably between Phe[16] and Trp[37]) resulting from the kink induced by the Pro[31] residue in the [29]RAPRKKG[35] linker. This latter point was further confirmed by the substitution of Pro[31] with D-Pro[31] in a synthetic analogue, which led to the disappearance of the long range NOEs between the two fingers and a severe reduction in the *in vitro* dimerization activity (Morellet et al., 1994).

To further investigate the spatial proximity of NCp7 zinc finger motifs, which is probably critical in the nucleic acid-binding mechanism of NCp7, steady-state and time-resolved fluorescence parameters for both the native Trp[37] (in the COOH-terminal finger motif) and the conservatively substituted Trp[16] (in the NH_2-terminal finger motif) were determined, and the distance between the residues in positions 16 and 37 was measured directly by Tyr-Trp fluorescence resonance energy transfer (FRET) measurements. These data were compared to those obtained on negative control derivatives with Pro[31] substituted by D-Pro[31] or with an altered NH_2-terminal finger motif. Taken together, our data clearly support the spatial proximity of NCp7 zinc finger motifs.

MATERIALS AND METHODS

Solid phase synthesis of (12–53)NCp7 and related peptides (Figure 1) was carried out as previously described (De Rocquigny et al., 1991). To preserve the highly oxidizable cysteine residues, the lyophilized peptides were stored under vacuum. Prior to use, they were dissolved in freshly degassed 50 mM Hepes/100 mM KCl (pH 7.5) buffer and immediately poured into anaerobic quartz cells, which maintained an inert argon atmosphere.

Absorption spectra were recorded on a Cary 4 spectrophotometer. Extinction coefficients of 5700 and 7000 M^{-1} cm^{-1} at 280 nm were used to determine the concentration of Tyr-lacking and Tyr-containing peptides, respectively.

Fluorescence spectra were performed at 20 ± 0.5 °C with an SLM 48000 spectrofluorometer. Quantum yields were determined by taking L-Trp in water ($\phi = 0.14$) as a reference (Eisinger & Navon, 1969).

Fluorescence lifetime measurements were performed using the time-correlated, single-photon-counting technique. The output of a Spectra-Physics mode-locked argon laser was used to synchronously pump a rhodamine 6G dye laser that was cavity dumped at 0.8 MHz and frequency doubled. Fluorescence excitation was at 295 nm, with emission collected at 350 nm through a 4 nm band-pass monochromator (Jobin-Yvon H10) combined with a Schott WG320 cutoff filter to eliminate the residual diffusion of the excitation light. The single-photon pulses were detected by a microchannel plate Hamamatsu R3809U photomultiplier coupled to a Phillips 6954 pulse preamplifier and recorded on a multichannel analyzer (Ortec 7100) calibrated at 26.5 ps/channel. The instrumental response function was recorded with a polished aluminum reflector, and its full width at half-maximum was 50 ps. The decay data were analyzed as a sum of exponentials: $I(t) = I_0\sum\alpha_i e^{-t/\tau_i}$ where $I(t)$ and I_0 are the intensities at times t and $t = 0$, respectively, α_i is the normalized preexponential term such as $\sum\alpha_i = 1$, and τ_i is the lifetime component. Analysis via this multiexponential form was performed by an iterative reconvolution procedure based on the estimated covariance matrix (Lami & Piémont, 1992). Since up to 20 decays were accumulated for each sample, confidence intervals of the mean recovered decay parameters were estimated using Hotelling's T^2 statistics. The number of exponentials was progressively increased until the fit did not improve. The adequacy of the fit was judged by reduced χ^2_R and by visual inspection of the weighted residuals and the autocorrelation function. As a general rule, only deconvolutions yielding a reduced χ^2_R value of $1 \pm 3(2/\nu)^{1/2}$, ν being the number of degrees of freedom, were retained. Typically a good fit was obtained if $0.8 \leq \chi^2_R \leq 1.2$.

Time-resolved anisotropy measurements were performed with the same device used for the intensity decay experiments. A complete description of these measurements has been reported elsewhere (Mély et al., 1993a). Briefly, the vertical and horizontal decays were alternately recorded over 30 s each, and after the recovery of the total fluorescence decay as a sum of exponentials, they were fitted according to $I_\parallel(t) = {}^1/_3 I_t(t)(1 + 2r(t))$ and $I_\perp(t) = {}^1/_3 I_t(t)(1 - r(t))$. The anisotropy decay $r(t)$ is given by $r(t) = \sum r_0\beta_i e^{-t/\theta_i} + r_\infty$, where $r_0\beta_i$ is the amplitude associated with the rotational correlation time, θ_i, and r_∞, is the infinite time anisotropy. Using the same procedure as was used for lifetime measurements, the mean parameter values and corresponding confidence intervals were calculated. In all cases, the confidence intervals of a given parameter obtained with $I_\parallel(t)$ and $I_\perp(t)$ overlap and r_∞ was found to be negligibly small.

Structure calculations were performed from ^{1}H NMR data of the (13–51)NCp7 peptide reported by Morellet et al. (1992). The experimental NOE intensities were converted into upper bond distance constraints and used as inputs for distance geometry calculations with the DIANA program (Güntert et al., 1991). The resulting conformers were then subjected to refinement through an energy minimization procedure with the AMBER program (Pearlman et al., 1991). Zinc force field parameters were introduced in the latter procedure in order to take into account the zinc ligand interactions (Jacob, 1990). The methodology as well as the description of the resulting three-dimensional structures will be published elsewhere. The graphic analyses were performed on an IRIS 4D35 workstation (Silicon Graphics Inc.), using the INSIGHT molecular modeling package (BIOSYM Technologies Inc.).

RESULTS

Strategy of Derivative Synthesis. Since both zinc finger motifs of NCp7 are characterized by a single aromatic amino acid (i.e., Phe[16] in the NH_2-terminal finger and Trp[37] in the COOH-terminal one) and since a close contact between these two residues has been depicted by Morellet et al. (1992), it was interesting to selectively monitor the fluorescence properties of these two residues. As Phe[16] is only weakly fluorescent, the wild-type (12–53)NCp7 (Figure 1) was used to monitor the properties of the Trp[37] residue, whereas the properties of the NH_2-terminal finger aromatic amino acid were investigated on a doubly substituted Trp[16]Phe[37] (12–53)NCp7 derivative. As the three-dimensional structures of the two NCp7 fingers were found to be largely superimposable (South et al., 1991), and as the residue immediately following the first Cys in the zinc finger motifs was indifferently Phe or Trp in various related NCs (Green & Berg, 1989), this double substitution was not expected to modify the structure of the peptide. Moreover, and most importantly, the distance between the residues in positions 16 and 37 was measured directly by Tyr-Trp FRET measurements on a Tyr[16] (12–53)NCp7 derivative.

To further assess the spatial proximity of the two fingers in NCp7, three negative control derivatives in which the fingers were not expected to be in close contact were synthesized. As substitution of Pro[31] with D-Pro[31] was reported to remove the spatial proximity between the two zinc finger motifs (Morellet et al., 1994), the fluorescence properties of Trp[37] and the

	Motif 1		Motif 2		
^{12}NVK	CFNCGKEGHTARNC	RAP RKKG	CWKCGKEGHQMKDC	TERQ^{53}	Wild Type (12-53)NCp7
---	-Y----------	--- ----	----------	----	Tyr^{16}(12-53)NCp7
---	-W----------	--- ----	-F----------	----	$Trp^{16}Phe^{37}$(12-53)NCp7
---	----------S	--- ----	----------	----	Ser^{28}(12-53)NCp7
---	-Y----------	--P*----	----------	----	Tyr^{16}D-Pro^{31}(12-53)NCp7
---	-W----------	--P*----	-F----------	----	Trp^{16}D-$Pro^{31}Phe^{37}$(12-53)NCp7

FIGURE 1: Amino acid sequences of (12–53)NCp7 derivatives. Motifs 1 and 2 correspond to the NH_2- and COOH-terminal zinc finger domains, respectively. P* refers to the D-Pro isomer. Underlined amino acids were replaced as indicated in the various mutants.

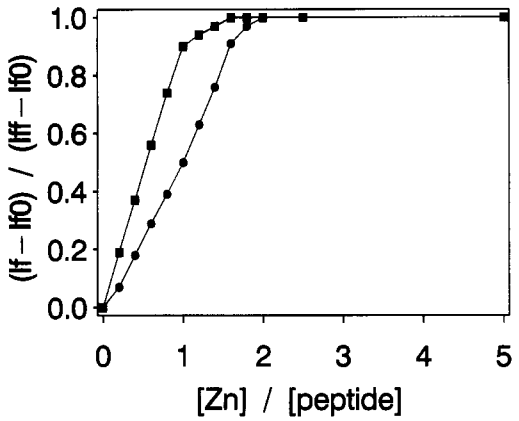

FIGURE 2: Zinc-binding curves of (12–53)NCp7 (●) and Ser^{28} (12–53)NCp7 (■). Protein concentrations were 10 μM. I_{fo}, I_f, and I_{ff} are the peptide fluorescence in the absence and in the presence of a given and a saturating zinc concentration, respectively.

interchromophore distance between the residues at positions 16 and 37 were determined on a doubly substituted Tyr^{16}D-Pro^{31} (12–53)NCp7. Moreover, similar to the native derivative, the properties of the aromatic amino acid in the NH_2-terminal finger were investigated on a triply substituted Trp^{16}D-$Pro^{31}Phe^{37}$ (12–53)NCp7 derivative. Finally, as it was shown that, in contrast to zinc-saturated peptides, apopeptides adopt a random coil conformation (Green & Berg, 1990), we synthesized a derivative with an altered NH_2-terminal finger to obtain a derivative with one finger motif being structured and the other one remaining random. This selective alteration was achieved by replacing Cys^{28} with Ser since a similar substitution in the related NCp10 of Moloney murine leukemia virus dramatically decreased the zinc affinity by a factor of 10^6 (Mély et al., 1991). The zinc-binding properties of this Ser^{28} (12–53)NCp7 derivative were compared to those of the wild-type by monitoring the fluorescence of Trp^{37}, which constitutes a sensitive probe of the saturation of the COOH-terminal finger. Clearly, the binding of zinc to (12–53)NCp7 reached a plateau for a zinc to peptide molar ratio of 2, suggesting that both fingers bind zinc competitively (Figure 2). In contrast, the binding of zinc to Ser^{28} (12–53)NCp7 was essentially complete for a zinc to peptide molar ratio of 1, suggesting that the COOH-terminal motif of this derivative was saturated first. Moreover, the 1D NMR spectra of this peptide, at a zinc to peptide molar ratio of 1, unambiguously indicated that the chemical shifts of the H-2 and H-4 protons of His^{44} in the COOH-terminal motif and His^{23} in the NH_2-terminal finger (Table 1) matched those of a zinc-complexed and noncomplexed His, respectively (Wüthrich, 1986), and that the COOH-terminal finger was folded, whereas the 12–33 residues were in a random coil conformation.

All of the derivatives were studied in the presence of saturating concentrations of zinc, except for Ser^{28} (12–53)-NCp7 where a zinc to peptide molar ratio of 1 was used.

Table 1: ^{1}H NMR Resonance Assignments of the Aromatic Histidine Protons in the (12–53)NCp7 and Ser^{28} (12–53)NCp7 Peptides[a]

	(12–53)NCp7[b]		Ser^{28} (12–53)NCp7[c]	
	H-2	H-4	H-2	H-4
His^{23}	7.41[d]	7.04	7.67	6.92
His^{44}	7.52	6.85	7.52	6.84

[a] Experiments were performed in D_2O at pH 7.11, 298 K, and a molar ratio of zinc to peptide of [b] 2.5 and [c] 1. [d] Chemical shift values are given relative to tetramethylsilane referenced to internal H_2O and expressed in ppm. Chemical shift values are typically accurate to ±0.01 ppm.

Quantum Yields and Fluorescence Resonance Energy Transfer. The emission spectra of the various peptides were qualitatively similar, with a maximum emission wavelength at 353 ±1 nm in keeping with a full exposition of both Trp^{16} and Trp^{37} to the aqueous solvent. In contrast, the comparison of their quantum yields (Tables 2 and 3) clearly revealed the existence of two classes for either Trp^{16} or Trp^{37}: a high quantum yield class, comprising all of the negative control derivatives [Ser^{28} (12–53)NCp7, Tyr^{16}D-Pro^{31} (12–53)NCp7, and Trp^{16}D-$Pro^{31}Phe^{37}$ (12–53)NCp7], and a lower quantum yield class, comprising the derivatives with putatively interacting fingers.

From the Tyr-containing peptides [Tyr^{16} (12–53)NCp7 and Tyr^{16}D-Pro^{31} (12–53)NCp7], the energy transfer efficiency, E, between Tyr^{16} and Trp^{37} was recovered from the steady-state acceptor (Trp^{37}) fluorescence enhancement according to

$$E = (\phi_{Trp280}/\phi_{295} - f_{Trp280})/f_{Tyr280}$$

where f_{Tyr280} and f_{Trp280} are the fractional absorptions of Tyr and Trp, respectively, while ϕ_{Trp280} and ϕ_{295} are the measured quantum yields of Trp at 280 and 295 nm excitation wavelengths, respectively. ϕ_{Trp280} was deduced from the measured quantum yield ϕ_{280} using $\phi_{Trp280} = \phi_{280}(S_{Trp280}/S_{280})$, where S_{280} is the area under the curve of the whole emission spectrum and S_{Trp280} is that of the emission spectrum obtained by normalizing, at 380 nm (where only Trp fluoresces), the emission spectra corresponding to excitation at 280 and 295 nm, respectively (Figure 3). Highly reproducibly, the quenching efficiency of Tyr^{16} (12–53)NCp7 was found to be about twice that of Tyr^{16}D-Pro^{31} (12–53)NCp7 (Table 4). Using these quenching efficiencies, we further characterized these Tyr-containing peptides by calculating the quantum yield, ϕ_D, of the donor (Tyr^{16}) in the absence of the acceptor, using

$$\phi_D = \phi_{DA}/(1 - E)$$

Table 2: Fluorescence Quantum Yields and Decay Parameters of Trp^{37}-Containing (12–53)NCp7 Derivatives[a]

peptide	ϕ_{295}	n	τ_i (ns)	α_i (%)	χ_R^2	$\langle\tau\rangle$ (ns)	$\phi_{295}/\langle\tau\rangle$ (s^{-1})
(12–53)NCp7		2[b]	6.4	57	1.7[c]		
			1.2	43			
	0.185 (±0.003)	3	6.79 (±0.07)	45 (±1)	1.05	3.7	5.0×10^7
			1.8 (±0.1)	35 (±1)			
			0.18 (±0.06)	20 (±3)			
Tyr^{16} (12–53)NCp7		2	6.2	62	1.6		
			1.3	38			
	0.182 (±0.004)	3	6.5 (±0.1)	42 (±2)	1.05	3.3	5.5×10^7
			1.7 (±0.2)	28 (±2)			
			0.16 (±0.08)	30 (±3)			
Tyr^{16}D-Pro^{31} (12–53)NCp7	0.240 (±0.004)	2	6.6 (±0.1)	58 (±2)	1.1	4.6	5.2×10^7
			1.8 (±0.1)	42 (±2)			
Ser^{28} (12–53)NCp7	0.217 (±0.007)	2	6.4 (±0.2)	54 (±2)	1.05	4.3	5.0×10^7
			1.8 (±0.2)	46 (±2)			

[a] The peptide concentrations were about 10 μM. Excitation and emission wavelengths were 295 and 350 nm, respectively. Lifetime components τ_i and normalized preexponential terms α_i are expressed as means (±confidence intervals at the 5% level of significance). The mean fluorescence lifetime is calculated using $\langle\tau\rangle = \sum\alpha_i\tau_i$. [b] n designates the number of exponential components. [c] A good fit was obtained only if $0.8 \leq \chi_R^2 \leq 1.2$, as described under Materials and Methods. The use of a single exponential to fit the data gave a χ_R^2 greater than 5 in each case.

Table 3: Fluorescence Quantum Yields and Decay Parameters of Trp^{16}-Containing (12–53)NCp7 Derivatives[a]

peptide	ϕ_{295}	n	τ_i (ns)	α_i (%)	χ_R^2	$\langle\tau\rangle$ (ns)	$\phi_{295}/\langle\tau\rangle$ (s^{-1})
$Trp^{16}Phe^{37}$ (12–53)NCp7		2	4.7	45	3.2		
			0.8	55			
	0.124 (±0.004)	3	5.40 (±0.04)	29 (±1)	1.05	2.2	5.6×10^7
			1.48 (±0.07)	36 (±2)			
			0.18 (±0.02)	35 (±2)			
Trp^{16}D-$Pro^{31}Phe^{37}$ (12–53)NCp7	0.183 (±0.004)	2	5.52 (±0.02)	69 (±1)	1.05	4.2	4.4×10^7
			1.16 (±0.03)	31 (±1)			

[a] Peptide concentrations, symbols, and expression of results are as in Table 2.

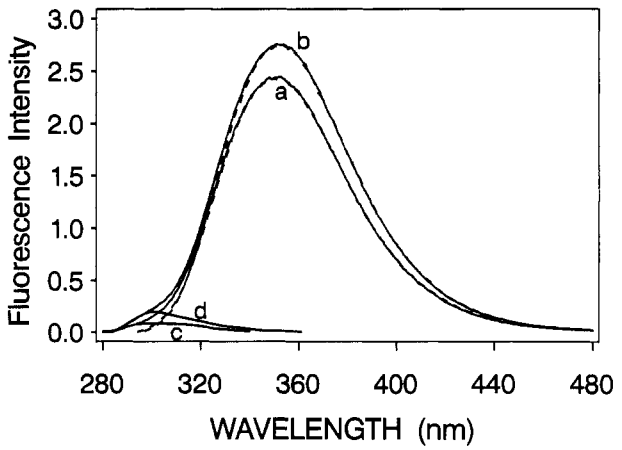

FIGURE 3: Fluorescence spectra of Tyr^{16} (12–53)NCp7 and Tyr^{16}D-Pro^{31} (12–53)NCp7. The spectra of Tyr^{16} (12–53)NCp7 (a) and Tyr^{16}D-Pro^{31} (12–53)NCp7 (b) obtained for excitation at 280 (—) and 295 nm (- - -) were normalized at 380 nm, where fluorescence originates only from tryptophan. The difference spectra (c and d) correspond to the residual emission of the Tyr^{16} residue in Tyr^{16} (12–53)NCp7 (c) and Tyr^{16}D-Pro^{31} (12–53)NCp7 (d).

where ϕ_{DA}, the quantum yield of the donor in the presence of the acceptor, was determined from Figure 3 by $\phi_{DA} = (1 - S_{Trp280}/S_{280})(\phi_{280}/f_{Tyr280})$. A dramatic decrease in ϕ_D was clearly observed for Tyr^{16} (12–53)NCp7 compared to Tyr^{16}D-Pro^{31} (12–53)NCp7 (Table 4). Thus, irrespective of the amino acid in position 16, a higher quenching environment was achieved in the derivatives with putatively interacting fingers.

Time-Resolved Intensity Decays. The fluorescence decay parameters, obtained by a time-correlated, single-photon-counting technique, of both Trp^{37}- and Trp^{16}-containing peptides are presented in Tables 2 and 3, respectively. As with fluorescence quantum yields, the same two classes could be distinguished for either Trp^{16} or Trp^{37}. The first class, comprising the negative control derivatives, could be adequately fit with a major long-lived fluorescence lifetime and a minor shorter one. The addition of a third component did not improve the accuracy of the fit. In contrast, the fluorescence decay of the derivatives with putatively interacting fingers could not be adequately fit by a biexponential function, but needed an additional subnanosecond component (Figure 4, Tables 2 and 3). This short component was highly reproducible and, due to the high resolution of our time-resolved device (characterized by an instrumental response full width at half-maximum (fwhm) of 50 ps), highly significant. Moreover, the appearance of this short lifetime induced a sharp decrease in the mean fluorescence lifetime that was fully consistent with the decrease in fluorescence quantum yield, as could be seen from the comparison of the $\phi/\langle\tau\rangle$ ratios. Indeed, irrespective of the geometry of the finger motifs, the $\phi/\langle\tau\rangle$ ratio of both Trp^{16} and Trp^{37} corresponded, as expected, to the radiative rate constant of a fully solvent-exposed Trp residue (Werner & Forster, 1979).

Time-Resolved Anisotropy Measurements. As in the interacting finger model, the close proximity of Phe^{16} and Trp^{37} was expected to hinder the rotational motion of both residues, the time-correlated anisotropy decays of the various (12–53)NCp7 derivatives were investigated. In each derivative, the anisotropy decay $r(t)$ could be adequately fit by a biexponential function with a long correlation time, corresponding to the overall rotational diffusion of the peptide, and a short subnanosecond correlation time, corresponding to the Trp local motion (Table 5). Whereas no significant differences could be observed for the rotational correlation times themselves, the peptides with putatively interacting finger motifs differed from the other derivatives by the significantly higher amplitude, $r_0\beta_1$, associated with the long rotational correlation times of both Trp^{16} and Trp^{37}. Since $r_0\beta_1$ also describes the anisotropy remaining after the fast motion is

Table 4: FRET Parameters of Tyr^{16} (12–53)NCp7 and Tyr^{16}D-Pro^{31}(12–53)NCp7[a]

peptide	E	ϕ_D	$\langle\kappa^2\rangle$	R_0 (Å)	R (Å)
Tyr^{16} (12–53)NCp7	0.74 (±0.05)	0.020 (±0.005)	0.15–2.8	8.5–14	7–12
Tyr^{16}D-Pro^{31} (12–53)NCp7	0.31 (±0.04)	0.052 (±0.003)	0.25–2.3	11–16	12.5–18

[a] The peptide concentrations were about 10 μM. Transfer efficiency, E (calculated from Trp^{37} fluorescence enhancement, as described in the text), and Tyr quantum yield (in the absence of acceptor), ϕ_D, are expressed as means (±standard error of the mean) for at least 10 experiments. Lower and upper limits of $\langle\kappa^2\rangle$ and the Förster critical (R_0) and interchromophore (R) distances were calculated as described in the text.

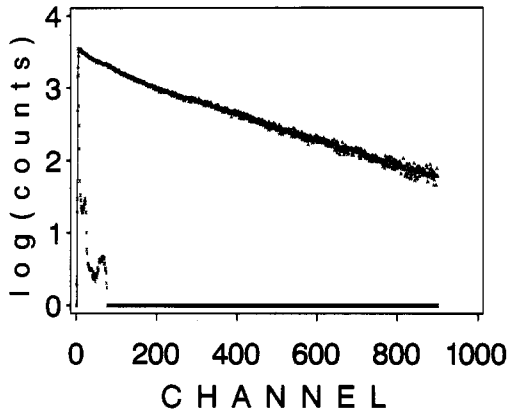

FIGURE 4: Total fluorescence intensity decay of (12–53)NCp7. Data were recorded by the single-photon-counting method. Excitation and emission wavelengths were 295 and 350 nm, respectively. The solid line is the computed curve of the (12–53)NCp7 intensity decay reconvolved using the optimal triexponential fit.

Table 5: Anisotropy Decay Parameters of (12–53)NCp7 Derivatives[a]

peptide	θ_i (ns)	$r_0\beta_i$	r_f	$\langle d\rangle$[b]
(12–53)NCp7	2.0 (±0.3)	0.14 (±0.01)	0.26	0.54
	0.13 (±0.05)	0.12 (±0.06)		
Tyr^{16} (12–53)NCp7	1.9 (±0.4)	0.14 (±0.01)	0.26	0.54
	0.15 (±0.1)	0.10 (±0.06)		
Tyr^{16}D-Pro^{31} (12–53)NCp7	2.2 (±0.4)	0.10 (±0.01)	0.26	0.38
	0.3 (±0.1)	0.13 (±0.04)		
Ser^{28} (12–53)NCp7	2.0 (±0.2)	0.10 (±0.01)	0.26	0.38
	0.2 (±0.1)	0.14 (±0.04)		
$Trp^{16}Phe^{37}$ (12–53)NCp7	2.2 (±0.3)	0.16 (±0.01)	0.27	0.59
	0.10 (±0.06)	0.11 (±0.06)		
Trp^{16}D-$Pro^{31}Phe^{37}$ (12–53)NCp7	2.2 (±0.3)	0.11 (±0.01)	0.27	0.41
	0.20 (±0.04)	0.14 (±0.06)		

[a] Experimental conditions were as described for Table 2. The rotational correlation time, θ_i, its amplitude, $r_0\beta_i$, and the fundamental anisotropy, r_f, were determined as described in the text. [b] The depolarization factor $\langle d\rangle$ is given by $\langle d\rangle = r_0\beta_1/r_f$ (Dale et al., 1979).

complete, our data suggest that the local motion of both Trp^{16} and Trp^{37} was more constrained in the peptides with putatively interacting finger motifs. To further investigate this point, the fundamental anisotropies, r_f, of Trp^{16} and Trp^{37} were measured at −80 °C in a 90:10 (v:v) glycerol/buffer mixture. In this solvent mixture, the peptides remained bound to zinc, and thus, at least partly folded since the addition of EDTA largely decreased their fluorescence intensities. The measured fundamental anisotropies at 295 nm (Table 5) were in good agreement with the r_f value of Trp in propylene glycol at −70 °C (Valeur & Weber, 1977) and with the apparent initial anisotropy ($r(0) = \sum r_0\beta_i$) recovered from the anisotropy decay data. In keeping with our previous conclusion, a ca. 40% increase in the depolarization factor, $\langle d\rangle$, was observed for both Trp^{16} and Trp^{37} in the negative control derivatives (Table 5).

Interchromophore Distance Calculation. Using FRET and time-resolved anisotropy decay data, the distance, R, between Tyr^{16} and Trp^{37} could be calculated in both Tyr^{16} (12–53)-NCp7 and the negative control derivative, Tyr^{16}D-Pro^{31}(12–53)NCp7. Due to the dynamic nature of proteins, the distance between two chromophores is best described by a distribution of distances rather by a single distance. The recovery of this distribution could be obtained either from the time-resolved donor emission decay or from steady-state measurements in the presence of external quenchers [for a review, see Cheung (1991)]. Both methods focused on the donor fluorescence, but unfortunately in our derivatives, the very low fluorescence of Tyr^{16} compared to Trp^{37} and the inability to excite it selectively precluded such analyses. Thus, only a single distance R could be recovered from the steady-state acceptor (Trp^{37}) fluorescence enhancement. This method is still of interest, as it has been shown that distances recovered by this method are in good agreement with the average distance recovered from measurements of distance distribution and from X-ray data (Cheung, 1991; Wu & Brand, 1992). The main problem in determining R arises from the determination of the orientation factor κ^2, which can vary from 0 to 4, leading to large errors in distance measurement. To reduce the uncertainty in κ^2, time-resolved anisotropy data were used according to Dale et al. (1979). The Tyr^{16}-containing derivatives were used to provide information on the orientational freedom of the acceptor (Trp^{37}), whereas, due to the low fluorescence properties of Tyr^{16}, the orientational freedom of the donor was determined on the conservatively substituted Trp^{16} residue in the Trp^{16}-containing derivatives.

From the very rapid local motion of the indole moiety of both Trp^{16} and Trp^{37} (Table 5), we deduced that all possible orientations of both transition moments are explored many times during the transfer period and, thus, that the dynamic averaging conditions are met. Moreover, if we make the reasonable assumption that the orientational distributions of both donor and acceptor transition moments are axially symmetrical, the upper and lower limits of the dynamic average orientation factor , $\langle\kappa^2\rangle$, could be obtained using

$$\langle\kappa^2\rangle_{max} = {}^2/_3[1 + \langle d_D^x\rangle + \langle d_A^x\rangle + 3\langle d_D^x\rangle\langle d_A^x\rangle]$$

and

$$\langle\kappa^2\rangle_{min} = {}^2/_3\{1 - [(\langle d_D^x\rangle + \langle d_A^x\rangle)/2]\}$$

where the axial depolarization factors for the donor, $\langle d_D^x\rangle$, and the acceptor, $\langle d_A^x\rangle$, are given by the square root of the depolarization factors in Table 5.

The $\langle\kappa^2\rangle$ limits (Table 4) were then used to calculate the Förster critical distance according to $R_0^6 = (8.79 \times 10^{-25})\langle\kappa^2\rangle n^{-4}\phi_D J_{AD}$ (Eisinger et al., 1969), where the overlap integral $J_{AD} = 4.8 \times 10^{-16}$ M^{-1} cm^6, the refractive index n = 1.335, and the quantum yield ϕ_D of the donor in the absence of the acceptor was taken from Table 4. Finally, the interchromophore distance between residues in positions 16 and 37 was calculated from R_0 and the energy transfer efficiency, E, according to $R = R_0[(1/E) - 1]^{1/6}$. The interchromophore distance ranges of the two peptides (Table 4) were clearly mutually exclusive: much shorter distances

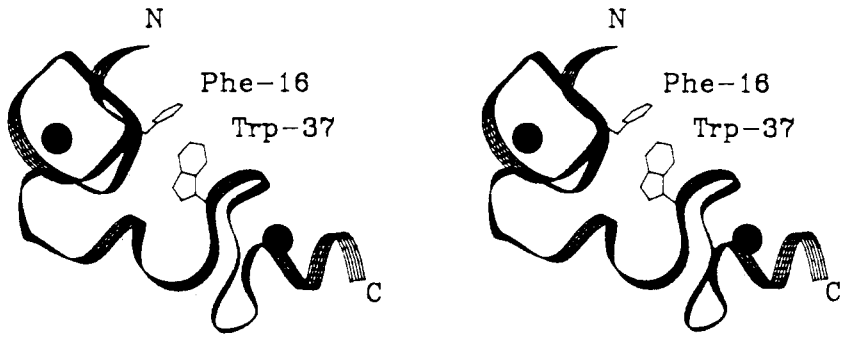

FIGURE 5: Stereoview of the wild-type (13–51)NCp7 structure: interacting finger model. The α carbon trace is shown by a thick ribbon, and the zinc atoms are depicted by their van der Waals spheres. The Phe[16] and Trp[37] aromatic residues are shown by a thin line following their side chain.

were obtained for the peptide with putatively interacting fingers.

DISCUSSION

Using either Trp[16] or Trp[37] as a fluorescent reporter of the NH_2- and COOH-terminal zinc finger motifs, respectively, we have reinvestigated the putative spatial proximity between the two finger motifs in the HIV-1 nucleocapsid protein. For this purpose, the fluorescent properties of the wild-type (12–53)NCp7 and two conservatively substituted derivatives with putatively interacting finger motifs were compared to those of three derivatives with either Pro[31] substituted by D-Pro[31] or an altered apo-NH_2-terminal zinc finger motif as negative controls. The fluorescence quantum yield, the intensity decay parameters, and the local mobility of both Trp[16] and Trp[37] in the negative control derivatives were largely similar to those of peptides with the amino acid sequences of the isolated NH_2- and COOH-terminal zinc finger domains, respectively (Mély et al., 1993b). As the Trp fluorescence parameters were critically dependent on their environment, this suggested that the environment of both Trp[16] and Trp[37] in the negative control derivatives was similar to that in the isolated zinc finger domains and thus was not modified at all by the complementary finger motif or the [29]RAPRKKG[35] linker sequence. Moreover, as the interchromophore distance directly measured by FRET was rather high in these derivatives, we concluded that the aromatic amino acids of both finger domains were far from each other and not in close contact with another part of the complementary finger motif or with the linker sequence.

In clear contrast, the fluorescence properties of both Trp[16] and Trp[37] were strongly modified in the derivatives with putatively interacting fingers since a more constrained mobility of the indole moiety and a sharp quantum yield decrease, correlated to the appearance of an additional subnanosecond lifetime, were observed. Moreover, a similar fluorescence quantum yield decrease was observed when Trp[16] was replaced with a Tyr residue. Both the simultaneous perturbation of the aromatic residues at positions 16 and 37 by the presence of the complementary zinc finger domains and the close interchromophore distance measured by FRET were clearly inconsistent with either an extended conformation (with a 28 Å interchromophore distance) or a random orientation of the finger domains (Omichinski et al., 1991; Summers et al., 1992). In contrast, our data were in full agreement with the spatial proximity of the zinc finger domains (Morellet et al., 1992), which could readily explain the decreased Trp mobility and the existence of an additional subnanosecond lifetime due either to additional collisions or radiationless relaxation processes if either the conformer (Szabo & Rayner, 1980) or the energy transfer model (Bajzer & Prendergast, 1993), respectively, were adopted.

To further validate the proximity of the zinc finger domains, some angular information on the 3D structure proposed by Morellet et al. (1992) was used to refine $\langle\kappa^2\rangle$ and thus the interchromophore distance range calculated by FRET. This approach is unbiased since only NMR-derived angles and not distances were used for calculations. The more general formula of $\langle\kappa^2\rangle$ is given by

$$\langle\kappa^2\rangle = (\kappa^x)^2\langle d_D^x\rangle\langle d_A^x\rangle + {}^1/_3(1 - \langle d_D^x\rangle) + {}^1/_3(1 - \langle d_A^x\rangle) + \cos^2\theta_D\,\langle d_D^x\rangle(1 - \langle d_A^x\rangle) + \cos^2\theta_A\,\langle d_A^x\rangle(1 - \langle d_D^x\rangle)$$

with $(\kappa^x)^2 = (\sin\theta_D \sin\theta_A \cos\Phi - 2\cos\theta_D \cos\theta_A)^2$. θ_D and θ_A represent the angles between the vector **R** joining the two chromophores and the symmetry axes $\mathbf{D^x}$ and $\mathbf{A^x}$ of the orientational distributions of donor and acceptor transition moments, respectively, whereas Φ represents the angle between the $(\mathbf{D^x},\mathbf{R})$ and the $(\mathbf{A^x},\mathbf{R})$ planes. These three angles are related to the θ_T angle between $\mathbf{D^x}$ and $\mathbf{A^x}$ by $\cos^2\theta_T = (\sin\theta_D \sin\theta_A \cos\Phi + \cos\theta_D \cos\theta_A)^2$. These angles could be readily obtained from the model of interacting fingers (Figure 5), but two intrinsic properties of Tyr and Trp complicate this task to some extent. The first is the probable existence of preferential χ^1 angles about the C^α–C^β bond for both Tyr[16] and Trp[37] (Schrauber et al., 1993). As the conformations with these preferential χ^1 angles correspond to low-energy stable conformations, molecular modeling using NMR data is expected to reconstitute some of them (at least the preferential ones). From the 18 lowest-energy conformations of (13–51)NCp7, χ^1 angles of −58°, -104°, and −154° were found for the Phe[16] residue with frequencies of 14, 2, and 2, respectively. For the Trp[37] residue, χ^1 angles of +177°, −34°, and −155° were found with frequencies of 2, 1, and 15, respectively. Thus, by assuming that the χ^1 angles of the residues at positions 16 and 37 were predominantly −58° and −155°, respectively (Figure 5), the 10 NMR-derived conformations containing both of these angles were selected for calculating θ_A, θ_D, and θ_T.

The second complication arises from the existence of two low-lying singlet excited states designated ^1L_a and ^1L_b in both Tyr and Trp residues. In the case of Tyr, at 280 nm excitation wavelength the ^1L_b transition was reported to be the major one (Hooker & Schellmann, 1970), and thus its transition moment situated in the plane at 90° to the symmetry axis was used for angular calculation. For Trp, the situation is similar since the contribution of the ^1L_a transition moment (situated −38° from the longest axis in Trp) has been shown to be the major one (Valeur & Weber, 1977) and was thus used for calculation. Using these assumptions, the NMR-derived angles and the deduced $\langle\kappa^2\rangle$, R_0, and R values are reported

Table 6: Refinement of the Tyr^{16}–Trp^{37} Distance Using NMR-Derived Angles[a]

Φ	θ_D	θ_A	θ_T	$\langle\kappa^2\rangle$	R_0 (Å)	R (Å)
100.3	59.8	118.4	112.1	0.18	8.8	7.4
142.4	76.9	114.3	142.9	0.30	9.6	8.1
81.6	68.6	50.0	70.2	0.21	9.1	7.6
99.3	52.3	92.4	98.9	0.06	7.3	6.1
57.2	90.8	129.2	64.6	0.23	9.2	7.7
64.7	88.3	119.4	69	0.21	9.1	7.6
128.8	108.3	80.4	129.7	0.25	9.4	7.8
82.6	98.8	110.0	80.1	0.06	7.4	6.2
70.7	91.0	126.8	74.0	0.14	8.5	7.1
50.65	89.3	136.4	64.6	0.29	9.6	8.0

[a] Angles were measured on 10 selected NMR-based structures as described in the text. The average orientation factor, $\langle\kappa^2\rangle$, the Förster critical distance, R_0, and the Tyr^{16}–Trp^{37} distance, R, were calculated as described in the text.

in Table 6. The mean interchromophore distance deduced from this approach was 7.3 ± 0.7 Å, corresponding to the lower end of the distance range obtained from fluorescence data alone and in good agreement with the 5.7 ± 1.5 Å range deduced from NMR data (Morellet et al., 1992).

The slightly larger Tyr^{16}–Trp^{37} distances obtained by this approach compared to the Phe^{16}–Trp^{37} NMR measurements could tentatively be explained either by the partial inability of Tyr and Trp residues to model the Phe residue in position 16 or by the pH and protein concentration differences between the NMR and fluorescence experiments. Finally, our conclusions on the proximity of the zinc finger domains still held true, even if the ^1L_a and ^1L_b transition moments of Tyr^{16} and Trp^{37}, respectively, were not negligible or if conformations with different χ^1 angles intervened since, in these cases, a decrease in the $\langle\kappa^2\rangle$ range toward the isotropic dynamic average value of $^2/_3$ and therefore a slight increase in R toward 9 Å (still in reasonable agreement with the finger proximity) were expected. This spatial proximity must be of critical importance for an optimal interaction with specific domains of target nucleic acids, as it is suggested from the severe reduction of *in vitro* dimerization activity in a derivative where Pro^{31} was substituted by D-Pro^{31} (Morellet et al., 1994).

ACKNOWLEDGMENT

We are indebted to Professor H. Lami for his suggestions and help in lifetime measurements and to M. Wernert for her expert editorial assistance.

REFERENCES

Aldovini, A., & Young, R. A. (1990) *J. Virol. 64*, 1920–1926.
Bajzer, Z., & Prendergast, F. G. (1993) *Biophys. J. 65*, 2313–2323.
Barat, C., Lullien, V., Schatz, O., Keith, G., Nugeyre, M. T., Grüninger-Leitch, F., Barré-Sinoussi, F., Le Grice, S. F. J., & Darlix, J. L. (1989) *EMBO J. 8*, 3279–3285.
Barat, C., Le Grice, S. F. J., & Darlix, J. L. (1991) *Nucleic Acids Res. 19*, 751–757.
Berg, J. M. (1986) *Science 232*, 485–487.
Bess, J. W., Jr., Powell, P. J., Issaq, H. J., Schumack, L. J., Grimes, M. K., Henderson, L. E., & Arthur, L. O. (1992) *J. Virol. 66*, 840–847.
Cheung, H. C. (1991) in *Topics in Fluorescence Spectroscopy, Vol. 2: Principles* (Lakowicz, J. R., Ed.) pp 127–176, Plenum Press, New York.
Dale, R. E., Eisinger, J., & Blumberg, W. E. (1979) *Biophys. J. 26*, 161–194.
Darlix, J. L., Gabus, C., Nugeyre, M. T., Clavel, F., & Barré-Sinoussi, F. (1990) *J. Mol. Biol. 216*, 689–699.
De Rocquigny, H., Ficheux, D., Gabus, C., Fournié-Zaluski, M. C., Darlix, J. L., & Roques, B. P. (1991) *Biochem. Biophys. Res. Commun. 180*, 1010–1018.
De Rocquigny, H., Gabus, C., Vincent, A., Fournié-Zaluski, M. C., Roques, B. P., & Darlix, J. L. (1992) *Proc. Natl. Acad. Sci. U.S.A. 89*, 6472–6476.
Di Marzo Veronese, F., Rahman, R., Copeland, T. D., Oroszlan, S., Gallo, R. C., & Sarngadharan, M. G. (1987) *AIDS Res. Hum. Retroviruses 3*, 253–264.
Eisinger, J., & Navon, G. (1969) *J. Chem. Phys. 50*, 2069–2077.
Eisinger, J., Feuer, B., & Lamola, A. A. (1969) *Biochemistry 8*, 3908–3915.
Gorelick, R. J., Nigida, S. M., Bess, J. W., Jr., Arthur, L. O., Henderson, L. E., & Rein, A. (1990) *J. Virol. 64*, 3207–3211.
Green, L. M., & Berg, J. M. (1989) *Proc. Natl. Acad. Sci. U.S.A. 86*, 4047–4051.
Green, L. M., & Berg, J. M. (1990) *Proc. Natl. Acad. Sci. U.S.A. 87*, 6403–6407.
Güntert, P., Braun, W., & Wüthrich, K. (1991) *J. Mol. Biol. 217*, 517–530.
Hooker, T. M., Jr., & Schellman, J. A. (1970) *Biopolymers 9*, 1319–1348.
Jacob, O. (1990) Ph.D. Thesis, Université Louis Pasteur, Strasbourg, France.
Lami, H., & Piémont, E. (1992) *Chem. Phys. 163*, 149–159.
Mély, Y., Cornille, F., Fournié-Zaluski, M. C., Darlix, J. L., Roques, B. P., & Gérard, D. (1991) *Biopolymers 31*, 899–906.
Mély, Y., Rocquigny, H., Piémont, E., Déméné, H., Jullian, N., Fournié-Zaluski, M. C., Roques, B. P., & Gérard, D. (1993a) *Biochim. Biophys. Acta 1161*, 6–18.
Mély, Y., Piémont, E., Sorinas-Jimeno, M., Gérard, D., De Rocquigny, H., Jullian, N., Morellet, N., & Roques, B. P. (1993b) *Biophys. J. 65*, 1513–1522.
Morellet, N., Jullian, N., De Rocquigny, H., Maigret, B., Darlix, J. L., & Roques, B. P. (1992) *EMBO J. 11*, 3059–3065.
Morellet, N., De Rocquigny, H., Mély, Y., Jullian, N., Déméné, H., Ficheux, D., Gérard, D., Darlix, J. L., Fournié-Zaluski, M. C., & Roques, B. P. (1994) *J. Mol. Biol. 235*, 287–301.
Omichinski, J. G., Clore, G. M., Sakaguchi, K., Appella, E., & Gronenborn, A. M. (1991) *FEBS Lett. 292*, 25–30.
Pearlman, D. A., Case, D. A., Caldwell, J. C., Seibel, G. L., Singh, U. C., Weiner, P., & Kollman, P. A. (1991) AMBER 4.0, University of California, San Francisco.
Schrauber, H., Eisenhaber, F., & Argos, P. (1993) *J. Mol. Biol. 230*, 592–612.
South, T. L., Blake, P. R., Hare, D. R., & Summers, M. F. (1991) *Biochemistry 30*, 6342–6349.
Summers, M. F., South, T. L., Kim, B., & Hare, D. R. (1990) *Biochemistry 29*, 329–340.
Summers, M. F., Henderson, L. E., Chance, M. R., Bess, J. W., Jr., South, T. L., Blake, P. R., Sagi, I., Perez-Alvarado, G., Sowder, R. C., III, Hare, D. R., & Arthur, L. O. (1992) *Protein Sci. 1*, 563–574.
Szabo, A. G., & Rayner, D. M. (1980) *J. Am. Chem. Soc. 102*, 554–563.
Valeur, B., & Weber, G. (1977) *Photochem. Photobiol. 25*, 441–444.
Werner, T. C., & Forster, L. S. (1979) *Photochem. Photobiol. 29*, 905–914.
Wu, P., & Brand, L. (1992) *Biochemistry 31*, 7939–7947.
Wüthrich, K. (1986) in *NMR of protein and nucleic acids*, Wiley and Sons, New York.